THE ASTROPHYSICAL JOURNAL, 493:39–51, 1998 January 20

MEASURING HIGH-ORDER MOMENTS OF THE GALAXY DISTRIBUTION FROM COUNTS IN CELLS: THE EDGEWORTH APPROXIMATION

RITA SEUNG JUNG KIM AND MICHAEL A. STRAUSS[1]
Department of Astrophysical Sciences, Peyton Hall, Princeton University, Princeton, NJ 08544;
rita@astro.princeton.edu, strauss@astro.princeton.edu
Received 1997 January 21; accepted 1997 August 28

ABSTRACT

To probe the weakly nonlinear regime, past the point where simple linear theory is sufficient to describe the statistics of the density distribution, we measure the skewness (S_3) and kurtosis (S_4) of the count probability distribution function (CPDF) of the *IRAS* 1.2 Jy sample obtained from counts in cells. These quantities are free parameters in a maximum likelihood fit of an Edgeworth expansion convolved with a Poissonian to the observed CPDF. This method, applicable on scales $\gtrsim 5\ h^{-1}$ Mpc, is appreciably less sensitive to the tail of the distribution than are measurements of S_3 and S_4 from moments of the CPDF. We measure S_3 and S_4 to $l \sim 50\ h^{-1}$ Mpc; the data are consistent with scale invariance, yielding averages of $\langle S_3 \rangle = 2.83 \pm 0.09$ and $\langle S_4 \rangle = 6.89 \pm 0.68$. These values are higher than those found by Bouchet et al. in 1993 ($\langle S_3 \rangle = 1.5 \pm 0.5$ and $\langle S_4 \rangle = 4.4 \pm 3.7$) using the moments method on the same data set, owing to lack of correction for finite-volume effects in the latter work. Unlike the moments method, our results are quite robust to the fact that *IRAS* galaxies are underrepresented in cluster cores. We use N-body simulations to show that our method yields unbiased results.

Subject headings: galaxies: clusters: general — galaxies: statistics — infrared: galaxies — large-scale structure of universe — methods: numerical

1. INTRODUCTION

Many approaches have been used to characterize the clustering of galaxies, especially over the past decade as better and deeper redshift surveys have become available (see Borgani 1995 and Strauss & Willick 1995 for comprehensive reviews). The two-point correlation function and its Fourier transform, the power spectrum, which are the long popular methods for describing the clustering of galaxies, are complete statistical descriptions of the density field only if the phases of the Fourier modes of the density field are random. Indeed, simple inflationary models predict these random phases; if this condition holds, the one-point probability distribution function (PDF) of the density field, $\delta(\boldsymbol{r})$, is Gaussian.

As perturbations grow by gravitational instability, an initially Gaussian distribution remains Gaussian as long as the fluctuations remain in the linear regime. However, once nonlinear effects become important, the distribution deviates from its initial Gaussian state, and one needs higher order statistics to characterize the density field.

For a zero-mean Gaussian distribution, all reduced moments (cumulants) of the PDF are zero except the variance ($\langle \delta^2 \rangle \equiv \sigma^2$), hence nonzero skewness, $\langle \delta^3 \rangle$, kurtosis, $\langle \delta^4 \rangle - 3\sigma^4$, and higher order cumulants are measures of the deviation of the distribution from a Gaussian. In this paper, we consider only the two lowest order effects, the skewness and the kurtosis. These Nth-order cumulants are equal to the volume-averaged correlation functions,

$$\bar{\xi}_N(v) = \frac{1}{v^N} \int_v d^3\boldsymbol{r}_1\, d^3\boldsymbol{r}_2 \ldots d^3\boldsymbol{r}_N\, \xi_N(\boldsymbol{r}_1, \boldsymbol{r}_2, \ldots, \boldsymbol{r}_N)\,, \quad (1)$$

where $\bar{\xi}_2 \equiv \sigma_2 \equiv \langle \delta^2 \rangle$, $\bar{\xi}_3 \equiv \langle \delta^3 \rangle$, $\bar{\xi}_4 \equiv \langle \delta^4 \rangle - 3\sigma^4$, and so forth. Here the volume, v, over which the $\bar{\xi}_N$ are averaged is defined by the smoothing scale of the density field, δ.

[1] Alfred P. Sloan Foundation Fellow.

The assumption of scale invariance by Balian & Schaeffer (1988, 1989),

$$\xi_N(\lambda \boldsymbol{r}_1, \ldots, \lambda \boldsymbol{r}_N) = \lambda^{\gamma(N-1)} \xi_N(\boldsymbol{r}_1, \ldots, \boldsymbol{r}_N)\,, \quad (2)$$

yields the scaling relation,

$$\bar{\xi}_N(v) = S_N\, \bar{\xi}_2^{N-1}(v)\,, \quad (3)$$

where the quantities S_N are independent of scale. The scale invariance of S_N and the scaling relation (eq. [3]) are in fact predicted by perturbation theory in the mildly nonlinear regime, under the two assumptions of Gaussian initial conditions and growth of conditions via gravitational instability (Fry 1984a, 1984b; Bernardeau 1992). Thus, one can test the scale-invariance model by measuring the dependence of S_N on the smoothing scale, although it can be difficult in practice to rule out non-Gaussian models (Fry & Scherrer 1994; Bouchet et al. 1995).

Calculation of S_N from gravitational instability invokes $(N-1)$th order perturbation theory. Bernardeau (1994b) presents a method for calculating S_N for top-hat filters. The results are

$$S_3 = \tfrac{34}{7} - (n+3) \quad (4)$$

and

$$S_4 = \tfrac{60712}{1323} - \tfrac{62}{3}(n+3) + \tfrac{7}{3}(n+3)^2\,, \quad (5)$$

where n is the spectral slope of the power spectrum; a pure power-law spectrum is assumed. The expressions above are for $\Omega_0 = 1$; while the quantities S_N are sensitive to the slope of the power spectrum, the dependence on Ω_0 is quite weak (Bouchet et al. 1992, 1995). These and the corresponding results for a Gaussian filter have been confirmed with N-body simulations (Juszkiewicz, Bouchet, & Colombi 1993; Bernardeau 1994b; Łokas et al. 1995; Juszkiewicz et al. 1995). On the observational side, calculations of S_3 and S_4 have been done for the CfA (Huchra et al. 1983) and Southern Sky Redshift Survey (da Costa et al. 1991) cata-

logs by Gaztañaga (1992) and by Fry & Gaztañaga (1994) and on the *IRAS* 1.2 Jy sample (Fisher et al. 1995) by Bouchet et al. (1993; hereafter B93). Calculations of higher order angular moments have been done for the Lick galaxy counts (Szapudi, Szalay, & Boschan 1992), *IRAS* galaxies (Meiksin, Szapudi, & Szalay 1992), the Automatic Plate Measuring Facility (APM) galaxy survey (Gaztañaga 1994, 1995; Szapudi et al. 1995), and the Edinburgh/Durham Southern Galaxy Catalogue (Szapudi, Meiksin, & Nichol 1996). For optically selected galaxies, Gaztañaga (1992) found that $S_3 = 1.94 \pm 0.07$ up to a smoothing scale of ~ 22 h^{-1} Mpc, which is slightly higher than the value found by B93 for the *IRAS* sample: $S_3 = 1.5 \pm 0.5$.

The standard technique for measuring S_3 and S_4 from observational data involves calculation of the moments of the count probability distribution function (CPDF)[2] (§ 2.1), which in turn is determined via counts in cells. The high-order moments of the CPDF are of course weighted heavily by its high-density tail. Regions of such high density are rare, so these moments are highly sensitive to the presence or absence of a few clusters (Colombi, Bouchet, & Schaeffer 1994, 1995; Szapudi & Szalay 1996). Also, in a finite volume, there is always a densest region, and thus the CPDF goes to zero for higher densities. Not taking this finite-volume effect into account will cause the clustering amplitudes to be systematically underestimated. The CPDF asymptotes to an exponential at high densities, especially in the strongly nonlinear regime (Balian & Schaeffer 1989); one can thus extrapolate the observed CPDF to arbitrarily high densities. Thus one can obtain unbiased estimates of the high-order moments, *if the volume is large and dense enough to reach this asymptotic regime to allow the exponential to be fit* (Fry & Gaztañaga 1994; Colombi et al. 1994, 1995). This exponential asymptotic behavior is not expected for the weak regime, which makes it difficult to correct for finite-volume effects (see the discussion in B93). Finally, the tail of the distribution is also affected by *finite-sampling* effects; it can be underestimated if the CPDF is determined from too few spheres (Szapudi & Colombi 1996).

However, as we shall see, skewness and kurtosis affect the entire CPDF, not just the tails. In particular, skewness causes the mode of the distribution (the region where the measured CPDF is most robust) to shift from the mean. This motivates us to develop a new method of measuring the S_N from the CPDF, which is less sensitive to finite volume effects, by fitting the entire CPDF to a functional form.

There are several approaches to calculating the evolution of the PDF of δ from Gaussian initial conditions, using the Zeldovich (1970) approximation (Kofman et al. 1994) or Eulerian perturbation theory (Bernardeau 1992; Bernardeau & Kofman 1995; Colombi et al. 1997). The so-called Edgeworth expansion, which provides a convenient parametric form to account for small deviations from Gaussianity, gives an excellent fit to the PDF of δ in N-body models for small σ (Juszkiewicz et al. 1995). In this paper, we take the Edgeworth expansion convolved with a Poisson distribution as our model and perform a maximum likelihood fit with respect to the free parameters, S_N, to the observed CPDF of the *IRAS* 1.2 Jy survey from B93. We expect this method to be more robust than direct calculation of the moments, since it depends more on the overall shape of the distribution function than on the high-density tail region. Although there are several applications of the Edgeworth expansion to measure non-Gaussian statistics of the density field in the literature (Scherrer & Bertschinger 1991; Amendola 1994; Juszkiewicz et al. 1995), it has not yet been applied to observational data. We check the validity of our technique by applying it to *IRAS* mock catalogs taken from N-body simulations and compare the results with the predicted value of S_3 and S_4 from perturbation theory and with values measured from the moments of the PDF.

In § 2 we give a brief account of the moments method and describe our model based on the Edgeworth expansion. We test this method with N-body simulations in § 3. In § 4, we apply our method to the *IRAS* 1.2 Jy CPDF and compare our results with those of the moments method and perturbation theory. We summarize our results in § 5.

2. METHOD AND ANALYSIS

2.1. *Count Probability Distribution Function and Its Moments*

The CPDF $P_N(l)$ is defined as the fraction of randomly positioned spheres of radius l containing exactly N galaxies for a given volume-limited galaxy sample. Here we use the CPDF of *IRAS* galaxies from 10 volume-limited subsamples as calculated by B93 (see their Table 1). We place 10^6 random points in each subsample and count the number of galaxies in concentric spheres of different radii, l, from each point, considering only those spheres that are completely included within the subsamples (see B93 for details).

B93 calculate the normalized cumulants S_N by the *moments method*. The moments of the distribution $P_N(l)$ are given by

$$\mu_M(l) = \left\langle \left(\frac{N - \bar{N}}{\bar{N}} \right)^M \right\rangle = \sum_{N=0}^{\infty} \left(\frac{N - \bar{N}}{\bar{N}} \right)^M P_N(l) , \quad (6)$$

where $\bar{N} \equiv \langle N \rangle = \sum N P_N(l)$ is the mean number of galaxies in a sphere of size l. The first few volume-averaged correlation functions (reduced moments), corrected for shot noise, are given by (Peebles 1980)

$$\bar{\xi}_2(l) = \mu_2 - \frac{1}{\bar{N}} , \quad (7)$$

$$\bar{\xi}_3(l) = \mu_3 - 3\frac{\mu_2}{\bar{N}} + \frac{2}{\bar{N}^2} , \quad (8)$$

$$\bar{\xi}_4(l) = \mu_4 - 6\frac{\mu_3}{\bar{N}} - 3\mu_2^2 + 11\frac{\mu_2}{\bar{N}^2} - \frac{6}{\bar{N}^3} . \quad (9)$$

The skewness and kurtosis, S_3 and S_4, then follow from equation (3). These calculations were done by B93 for the *IRAS* redshift survey, and it was found that the scaling relation (eq. [3]) indeed holds very well (see Fig. 8 of B93). A fit of the data to $\log \bar{\xi}_N = C_N + D_N \log \bar{\xi}_2$ gives $D_3 = 1.96 \pm 0.06$ and $D_4 = 3.03 \pm 0.18$, where scale invariance predicts $D_N = N - 1$ (eq. [3]). All calculations are done in redshift space, but the S_N are quite insensitive to redshift space distortions, at least on mildly nonlinear scales (Bouchet et al. 1992; Lahav et al. 1993; Fry & Gaztañaga 1994; Hivon

[2] The PDF refers to the distribution function of the underlying continuous density field, δ, while the CPDF is the distribution function of the discretely sampled galaxy distribution.

et al. 1995). As mentioned in the previous section, no correction for finite-volume or finite-sampling effects have been carried out for these data.

2.2. *The Edgeworth Expansion*

The primordial density fluctuations are assumed to be Gaussian distributed, and as these fluctuations grow by gravitational instability, the PDF of δ deviates away from its initial Gaussian form, generating nonzero higher order moments. To the extent that the deviations from a Gaussian are small, it makes sense to write the PDF as an expansion around a Gaussian. The Edgeworth expansion is a rigorous way to do this, as described by Juszkiewicz et al. (1995).

We expand the PDF, here denoted by $p(v)$, where $\delta \equiv (\rho - \bar{\rho})/\bar{\rho}$, $v \equiv \delta/\sigma$, in terms of a Gaussian

$$\phi(v) = \frac{1}{\sqrt{2\pi}} \exp\left(\frac{-v^2}{2}\right) \tag{10}$$

and its derivatives. This is called the Gram-Charlier series (Cramér 1946),

$$p(v) = \phi(v)\left[c_0 - \frac{c_1}{1!} H_1(v) + \frac{c_2}{2!} H_2(v) + \cdots\right], \tag{11}$$

where the H_l are the Hermite polynomials, as given in Table 1. By the orthogonality of the H_l one obtains

$$c_l = (-1)^l \int_{-\infty}^{\infty} H_l(v) p(v) dv \; . \tag{12}$$

Therefore, the first few coefficients of equation (11) are given by

$$c_0 = 1 \; , \quad c_1 = c_2 = 0 \; , \quad c_l = (-1)^l S_l \sigma^{l-2} \; , \quad (3 \le l \le 5) \; ,$$
$$c_6 = S_6 \sigma^4 + S_3^2 \sigma^2 \; , \tag{13}$$

where the S_l are the normalized cumulants defined in equation (3). A reordering of the terms of the Gram-Charlier series gives a proper asymptotic expansion in σ, the Edgeworth series:

$$p(v) = \phi(v)\left\{1 + \frac{1}{3!} S_3 H_3(v)\sigma + \left[\frac{1}{4!} S_4 H_4(v) + \frac{10}{6!} S_3^2 H_6(v)\right]\sigma^2 + \mathcal{O}(\sigma^3)\right\} . \tag{14}$$

2.3. *A Model for the CPDF*

Equation (14) is a model for the underlying density distribution from which the galaxies are sampled, but it does not yet account for the discreteness of the galaxies. Owing to the finite number of galaxies in each sample, the observed CPDF is subject to Poisson noise, and we take this effect into account by convolving the Edgeworth expansion with a Poisson distribution (see Coles & Jones 1991).

We define the density contrast as $\delta \equiv (N - \langle N\rangle)/\langle N\rangle$. Let us rewrite the Edgeworth expansion to third order (second order in σ) as a function of δ,

$$E(\delta) = \frac{1}{\sqrt{2\pi}\sigma} e^{-\delta^2/2\sigma^2}\left\{1 + \frac{1}{6} S_3 \sigma H_3\left(\frac{\delta}{\sigma}\right) + \left[\frac{S_4}{24} H_4\left(\frac{\delta}{\sigma}\right) + \frac{S_3^2}{72} H_6\left(\frac{\delta}{\sigma}\right)\right]\sigma^2\right\} . \tag{15}$$

The expectation value of $P(N)$ at a given value of l is given by the convolution of equation (15) with a Poisson distribution,

$$\langle P(N)\rangle = \int d\delta E(\delta) F[N \,|\, N_\delta \equiv \langle N\rangle(\delta + 1)] \; , \tag{16}$$

where the Poisson distribution is

$$F(N \,|\, N_\delta) = \frac{N_\delta^N}{N!} e^{-N_\delta} \; , \tag{17}$$

the conditional probability of finding N points in a sphere when the true overdensity in that sphere is $\delta = (N_\delta - \langle N\rangle)/\langle N\rangle$.

The Edgeworth expansion is not positive definite; moreover, for values of σ approaching unity, it shows unphysical oscillations (Juszkiewicz et al. 1995; Ueda & Yokoyama 1996). However, when we convolve it with a Poisson distribution, the Edgeworth expansion becomes much better behaved. Figure 1 illustrates this with the observed CPDF for a volume-limited sample of *IRAS* galaxies (*circles*). The CPDF is normalized to the total number of spheres that fill the volume, M (eq. [18]), and the error bars are given by Poisson statistics, i.e., the square root of the value of the CPDF. The solid curve is the best fit of the model in equation (16) (using the method described below), while the dashed curve shows the underlying Edgeworth expansion (eq. [15]) with the same values of σ, S_3, and S_4. The dashed line goes negative and oscillates around the CPDF, while the solid line traces it nearly perfectly. This example has $\sigma = 0.77$. The dotted line is the result of performing a fit of the Edgeworth expansion with no Poisson noise term included. Not surprisingly, the σ is overestimated, and the model gives a very poor fit. Thus, for the sparse *IRAS* data we use in this paper, the Poisson noise term is absolutely essential in our model for the CPDF. Note that the Edgeworth expansion is no longer valid for $\sigma > 1$, and thus the example in Figure 1 represents the smallest scales on which we will apply it.

The observed CPDF, $P(N)$, and the model, $\langle P(N)\rangle$, are defined to be the *probability* that a sphere of size l contains N points. When we assume that a total of M spheres are placed randomly within the volume, then the *number* of spheres that contain exactly N points is $\tilde{P}(N) \equiv MP(N)$; we similarly define $\langle \tilde{P}(N)\rangle \equiv M\langle P(N)\rangle$. We would like M to represent the number of *statistically independent* spheres in order to allow us to define error bars on the observed $P(N)$, but it is not clear a priori how to measure this. The number of spheres placed within the volume, 10^6, is clearly an over-

TABLE 1

HERMITE POLYNOMIALS, $H_l(v)$

l	Polynomial
0.....	1
1.....	v
2.....	$v^2 - 1$
3.....	$v^3 - 3v$
4.....	$v^4 - 6v^2 + 3$
5.....	$v^5 - 10v^3 + 15v$
6.....	$v^6 - 15v^4 + 45v^2 - 15$

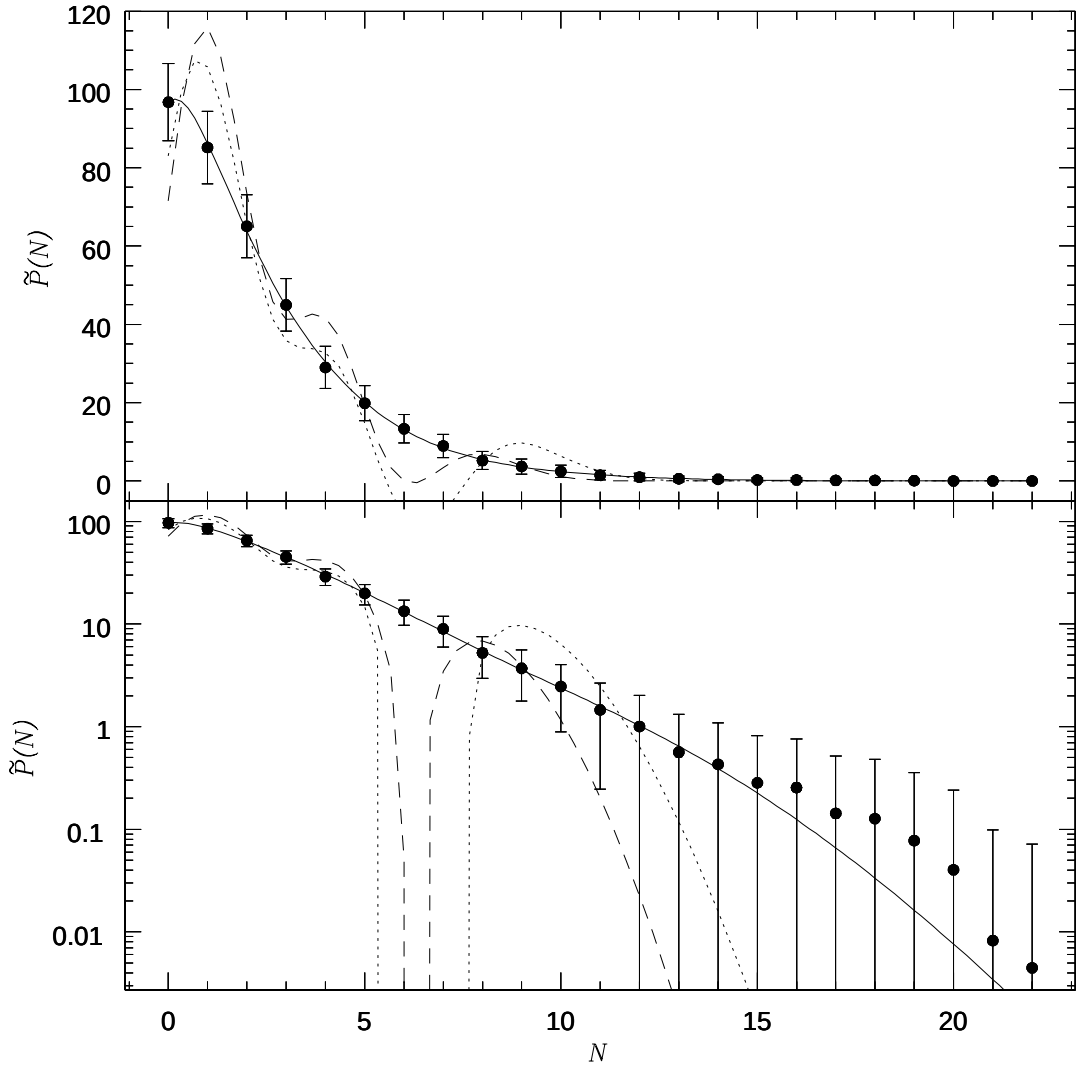

FIG. 1.—Comparison of the fit of the Edgeworth expansion convolved with a Poissonian (*solid line*) to the *IRAS* CPDF of sample size $R = 59\ h^{-1}$ Mpc and smoothing length $l = 7.92\ h^{-1}$ Mpc (*circles*), and the corresponding underlying density field (the pure Edgeworth expansion without shot noise component) (*dashed line*). The top panel is a linear plot, while the bottom has a logarithmic y-axis to better show the tail. The best-fit values of the parameters are $\sigma = 0.77$, $S_3 = 2.56$, and $S_4 = 7.38$. The dotted line is the result of a pure Edgeworth expansion fitted to the CPDF, without convolution with a Poissonian; the resulting parameters are $\sigma = 0.91$, $S_3 = 2.92$, and $S_4 = 12.95$.

estimate for M, owing to severe overlap between spheres.[3] One possibility, which is used to define error bars in Figures 1 and 2, is to take

$$M = \frac{\omega}{4\pi}\left(\frac{R}{l}\right)^3 , \tag{18}$$

the ratio of the volumes of the sample and the sphere;[4] here R is the radius of the subsample, and ω is the solid angle it subtends. However, Gaztañaga & Yokoyama (1993) show (and we confirm in § 2.4) that this is an underestimate, and they suggest multiplying equation (18) by σ^{-3} (which is much larger than unity on large scales). This issue is further discussed in Szapudi & Colombi (1996) and Szapudi et al. (1996). We do not have a rigorous solution to this problem. Our approach for the present paper is to use the value of M given by equation (18), demonstrate directly that it is an underestimate, and, in the following subsection, suggest an empirical rescaling to allow us to define error bars on measured quantities.

As explained above, we place 10^6 spheres in each volume to measure $P(N)$. This is multiplied by M, which is several orders of magnitude lower than 10^6, to obtain $\tilde{P}(N)$. We assume that this *number* of spheres, $\tilde{P}(N)$, is Poisson distributed around the true value $\langle\tilde{P}(N)\rangle$, so the likelihood of each observed data point, $\tilde{P}(N)$, is given by the Poisson distribution. We assume that the values of $\tilde{P}(N)$ are statistically independent (we will see in the following subsection that these assumptions appear to be violated but that we can make a heuristic fix to the likelihood). We therefore can express the likelihood function of the observed CPDF as the product of these quantities over N,

$$L = \prod_N \frac{\langle\tilde{P}(N)\rangle^{\tilde{P}(N)}}{\tilde{P}(N)!}\, e^{-\langle\tilde{P}(N)\rangle} . \tag{19}$$

In practice, the product extends only over those values of N for which $\tilde{P}(N) > 1$, as the Poisson model breaks down beyond that. Nevertheless, we will see that in many cases

[3] Note that 10^6 may be too *small* a number of spheres to avoid finite-sampling effects in the tails of the distribution; see Szapudi et al. (1996) and Szapudi & Colombi (1996). However, we argue below that the Edgeworth method is insensitive to such biases in the tail.

[4] Note that M, and accordingly $\tilde{P}(N)$, are not integers.

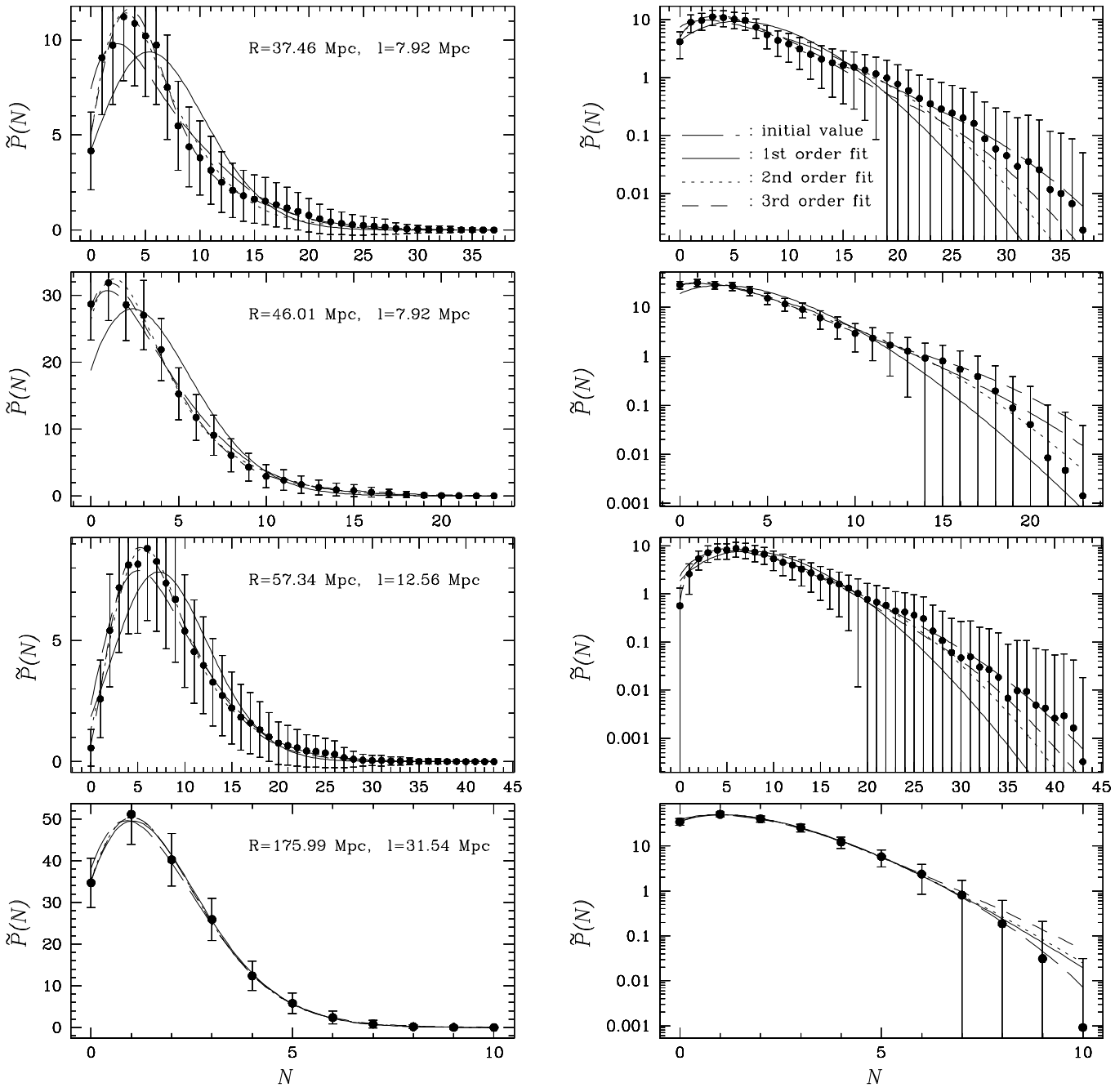

FIG. 2.—Various fits of the Edgeworth expansion convolved with a Poissonian to the observed CPDF (*circles*), with error bars given by Poisson statistics. R is the size of the *IRAS* sample, and l is the smoothing scale. The long-dashed line represents the model using the σ, S_3, and S_4 of the moments method, the solid line is our first-order fit, the dotted line is the second-order fit, and the short-dashed line the third-order fit. The volume of the subsample increases from top to bottom, and the solid line (Gaussian) becomes a better approximation. The right panels use a logarithmic y-axis to show the tails. The fits trace the data points reasonably well even when $\tilde{P}(N) < 1$, which were excluded in the likelihood analysis.

the best-fitting curve continues to trace the CPDF reasonably well, even when $\tilde{P}(N) < 1$ (see the right-hand panels of Fig. 2). We have assumed a Poisson distribution in $\tilde{P}(N)$; if we had assumed a Gaussian distribution, our likelihood function could be expressed in terms of χ^2. Here, the quantity corresponding to χ^2 is then

$$\mathscr{L} = -2 \ln L = \sum_N 2[\langle \tilde{P}(N) \rangle - \tilde{P}(N) \ln \langle \tilde{P}(N) \rangle + \ln (\tilde{P}(N)!)] , \quad (20)$$

and we minimize this quantity instead of maximizing L (eq. [19]). We use Powell's method (Press et al. 1992) to minimize $\mathscr{L}$ with respect to σ, S_3, and S_4; indeed, we do fits to first order (i.e., Gaussian), second order (including the term proportional to $S_3\sigma$), and third order in the Edgeworth expansion (eq. [15]), although we focus mainly on the third-order fit in this paper. To avoid having the code settle into a local minimum, we start the search with reasonable values of the parameters, i.e., those we calculate by the moments method. In most cases, this converges to a fair estimate of the parameters, but in some cases, especially on large scales, where the higher order correlations are intrinsically weak, or when the volume of the subsample is very large and hence the density of the galaxies are small, calculating the

moments yields negative quantities of S_3 and S_4. When this happens, we set the initial values of S_3 and S_4 to zero instead and minimize $\mathscr{L}$ again.

Maximum likelihood fits of first, second, and third order to the *IRAS* CPDFs for representative values of R and l are given in Table 2; those with asterisks are plotted in Figure 2. The left-hand panels of the figure give $\tilde{P}(N)$ on a linear scale to show the fit around the peak clearly. The right-hand panels are log plots that the tail region in detail. The error bars are again given by Poisson statistics as in Figure 1. The solid line is the first-order (Gaussian) fit, and the dotted line and the short dashed line represent second- and third-order fits, respectively. The second- and third-order fits are a remarkable improvement over the initial set of parameters obtained by the moments method, represented by the long-dashed lines. The third-order fits, with the term proportional to σ^2 included, are an improvement over the second-order fits. Note in particular that the third-order fits follow the observed CPDF even into the region where $\tilde{P}(N) < 1$, which is not even included in the fitting procedure. On the other hand, quite interestingly, the third-order model with the parameters given by the moments method (*long-dashed line*) usually does the best job of fitting the high-density tail of the CPDF, although this fit is poor at intermediate to low δ. This again reflects the sensitivity of the moments method to the tails of the distribution. As the volume of the subsample increases, going downward in the figure, the Gaussian fit becomes a better approximation to the observed CPDF. Indeed, for the bottommost panel with a subsample of volume 176 h^{-1} Mpc and a smoothing length of 31.54 h^{-1} Mpc, the first-, second-, and third-order fits are barely distinguishable. This is a result of two effects. First, the larger the subsample is, the sparser the sample becomes, and therefore the Poisson noise dominates the CPDF, swamping the higher order correlations. Second, the larger the smoothing scale, the weaker the higher order correlations become because clustering is weaker at larger scales. Therefore, in either of these cases, the accuracies of

TABLE 2

RESULTS OF REPRESENTATIVE FITS

Maximum Radius[a]	l[b]	$\bar{N}$[c]	Order	$\sigma(l)$	$S_3(l)$	$S_4(l)$	$\mathscr{L}$[d]
37.46[e]	7.92	6.57	m[f]	0.70	1.97	3.22	384.49
			1	0.61 ± 0.09	...	...	418.27
			2	0.56 ± 0.04	4.15 ± 0.83	...	369.02
			3	0.56 ± 0.05	3.17 ± 0.66	10.82 ± 4.08	363.01
46.01[e]	7.92	3.54	m	0.73	1.74	2.69	895.01
			1	0.68 ± 0.08	...	...	1050.8
			2	0.68 ± 0.04	2.70 ± 0.44	...	889.81
			3	0.78 ± 0.10	2.00 ± 0.28	6.80 ± 0.93	882.27
57.34	7.92	2.28	m	0.85	2.13	6.49	1187.2
			1	0.74 ± 0.06	...	...	1846.9
			2	0.73 ± 0.05	3.43 ± 0.56	...	1187.1
			3	0.77 ± 0.02	2.56 ± 0.11	7.38 ± 0.76	1170.6
57.34[e]	12.56	8.39	m	0.53	2.26	4.90	2066.3
			1	0.48 ± 0.08	...	...	2163.1
			2	0.46 ± 0.02	3.53 ± 0.57	...	2034.0
			3	0.45 ± 0.02	3.15 ± 0.32	7.83 ± 3.46	2033.9
72.35	7.92	0.98	m	0.81	1.30	1.12	701.67
			1	0.67 ± 0.06	...	...	1005.0
			2	0.74 ± 0.06	3.64 ± 0.79	...	527.17
			3	0.73 ± 0.02	2.85 ± 0.11	2.51 ± 1.94	499.30
72.35	12.56	3.82	m	0.54	1.32	4.35	140.29
			1	0.57 ± 0.08	...	...	142.70
			2	0.57 ± 0.02	1.39 ± 0.46	...	138.81
			3	0.52 ± 0.12	1.28 ± 0.80	−2.4 ± 14.5	138.63
90.02	7.92	0.45	m	0.87	1.63	1.34	1493.5
			1	0.58 ± 0.07	...	...	1635.6
			2	0.74 ± 0.06	4.69 ± 0.88	...	935.40
			3	0.76 ± 0.11	3.45 ± 0.66	9.17 ± 1.70	929.90
90.02	12.56	1.74	m	0.57	0.86	−3.6	253.78
			1	0.59 ± 0.08	...	...	268.85
			2	0.59 ± 0.02	2.01 ± 0.56	...	250.76
			3	0.58 ± 0.10	1.61 ± 0.73	1.44 ± 10.4	250.87
113.02	19.71	3.17	m	0.37	0.77	−21.6	357.50
			1	0.37 ± 0.07	...	...	353.54
			2	0.37 ± 0.03	3.40 ± 2.49	...	348.66
			3	0.33 ± 0.06	3.00 ± 1.96	−41.36 ± 100.8	347.29
175.99[e]	31.54	1.78	m	0.34	−0.38	−39.66	551.92
			1	0.35 ± 0.12	...	...	546.20
			2	0.35 ± 0.03	1.77 ± 0.94	...	545.30
			3	0.40 ± 0.16	1.93 ± 1.40	16.29 ± 13.6	544.77

[a] Radius of subsamples (h^{-1} Mpc).
[b] Radius of the sphere (h^{-1} Mpc).
[c] Average number of points in the sphere of size l.
[d] $\mathscr{L} = -2 \ln L$, L is likelihood; values shown here are scaled to the χ^2 per degree of freedom (see § 2.4).
[e] Examples shown in Fig. 2.
[f] Initial values of the fit, obtained by moments method.

the higher order correlation terms, S_3 and especially S_4, drop appreciably, and the error bars we derive for these quantities in the next section are therefore quite large.

2.4. *Error Estimates and the Value of M*

We determine errors on the parameters from the inverse of the Hessian matrix of the likelihood function. Close to the minimum, we expect the likelihood function to be well approximated by a quadratic form,

$$\mathscr{L}(\boldsymbol{x}) \approx \mathscr{L}(\boldsymbol{x}_0) + \tfrac{1}{2}(\boldsymbol{x} - \boldsymbol{x}_0) \cdot \boldsymbol{D} \cdot (\boldsymbol{x} - \boldsymbol{x}_0) , \qquad (21)$$

where $\boldsymbol{x}$ is the vector of parameters, and $\boldsymbol{x}_0$ is the value of this vector at the minimum value of $\mathscr{L}$. Here $\boldsymbol{D}$, the Hessian matrix, is the second-derivative matrix of $\mathscr{L}$. Since the form of the likelihood function is given, the Hessian matrix is known to us. The covariance matrix is then obtained by

$$[C] \equiv 2\boldsymbol{D}^{-1} , \qquad (22)$$

and $(C_{ii})^{1/2}$ are the 1 σ confidence intervals of the parameters x_i.

The values of the errors derived in this way are of course critically dependent on the value of M assumed. The third-order model fits the points in Figures 1 and 2 much too well, given the Poisson errors shown, which suggests that our value of M is underestimated. We can quantify this with a χ^2 statistic:

$$\chi^2 = \sum_N \frac{[\tilde{P}(N) - \langle \tilde{P}(N) \rangle]^2}{\tilde{P}(N)} , \qquad (23)$$

where Poisson error bars are assumed, and the sum is over only the $\mathscr{N}$ values of N for which $\tilde{P}(N) > 4$ (such that the correspondence between the Poisson distribution and the Gaussian distribution assumed in eq. [23] is valid). This quantity is less than the number of degrees of freedom, $\mathscr{N} - 4$, by factors of as much as 10. As we discussed in the previous subsection, it is not clear how to set M a priori, and consequently the errors on $P(N)$ and parameters derived from it (see the exhaustive discussion in Szapudi & Colombi 1996 for the strongly nonlinear regime; there does not yet exist a complete theory for the errors in the weakly nonlinear regime). We find that the Gaztañaga & Yokoyama (1993) suggestion of multiplying M by σ^{-3} does not bring $\chi^2/(\mathscr{N} - 4)$ to unity, although it does go in the right direction.

Our approach is an empirical one: we *scale* our errors of $\tilde{P}(N)$ to force $\chi^2 = \mathscr{N} - 4$; equivalently, we multiply the errors in σ, S_3, and S_4 derived above by $[\chi^2/(\mathscr{N} - 4)]^{1/2}$. This is done a posteriori and so does not affect the best-fit values of the parameters, but it does of course have a strong effect on the derived errors. This is not a statistically rigorous procedure, but we will justify these errors empirically in the next section. The 1 σ errors determined in this way are included in Table 2.

Table 2 includes the values of $\mathscr{L}$ for each fit; these have been scaled by the factor $\chi^2/(\mathscr{N} - 4)$. This way, one can quantify the goodness of fit of the curves seen in Figure 2 by comparing the relative likelihoods. The lower the value of $\mathscr{L}$, the better the fit becomes for given values of R and l; a difference of unity is significant at the 1 σ level. These values of $\mathscr{L}$ are not comparable across subsamples or smoothing scales, since in each case the input CPDF is different.

3. TESTS WITH *N*-BODY SIMULATIONS

To check the validity of our method, we generate *IRAS* mock catalogs from the N-body simulations of Protogeros & Weinberg (1997), kindly given to us by D. Weinberg. These assume an initial power spectrum, $P(k) \propto k^{-1}$, and $\Omega_0 = 0.3$, and are evolved forward to the point when σ_8, the rms fluctuation amplitude within an 8 h^{-1} Mpc sphere, is equal to 0.8. The simulations use a staggered mesh particle mesh code by Park (1990) and are evolved within a cube of size 300 h^{-1} Mpc, containing 150^3 particles and a 300^3 mesh. We assume that the galaxy distribution is unbiased relative to the dark matter. We choose a random point within the simulation to represent the Local Group, and produce 10 concentric, volume-limited, mock catalogs with exactly the same volumes and number densities as in the real universe (see also Table 1 of B93). We compute the CPDF for these samples with top-hat filters of the same radii as are used in the real universe and fit these to our Edgeworth model exactly as was done above. We wish to compare our results to the predictions of perturbation theory, and therefore work in real space, not in redshift space.

For Gaussian filters, N-body simulation checks for S_3 and S_4 (Juszkiewicz et al. 1993; Bernardeau 1994b; Łokas et al. 1995) have successfully matched the predicted values of S_3 and S_4 for the $n = -1$ power spectrum. The counts-in-cells method uses a top-hat filter, for which perturbation theory predicts $S_3^p = 2.86$ and $S_4^p = 13.89$ for the $n = -1$ power spectrum of our simulations, from equations (4) and (5).[5] Unlike the real *IRAS* data, biasing is not an issue we have to consider in the N-body simulations, and therefore we expect the perturbation theory prediction to agree quantitatively with the results of our method.

Figure 3 shows the values obtained for S_3 as a function of scale from the N-body model. Squares denote the weighted average of the values obtained by the third-order Edgeworth model to the CPDFs of the mock catalogs, at each scale. The data appear consistent with scale invariance, as indeed one expects for this power spectrum (see also the discussion in Colombi, Bouchet, & Hernquist 1996). Averaging over all scales gives $\langle S_3 \rangle = 2.93 \pm 0.09$ (*dotted line*), which is in beautiful agreement with the perturbation theory value (*solid line*).

The circles indicate the results of applying the moments method to the N-body simulation sampled at a density of 0.01 Mpc^{-3}. At this sampling density, the Poisson noise is relatively small, and the moments method yields an equal-weight average of $\langle S_3 \rangle = 2.90 \pm 0.64$, which is remarkably similar to the perturbation theory results and very much consistent with the Edgeworth approximation results of the mock catalogs. Note that the scatter around the mean of the determinations of S_3 using the moments method from the densely sampled data is appreciably larger than that of the Edgeworth expansion results based on the much sparser mock catalogs.

When we apply the moments method to the more sparsely sampled mock catalogs (Fig. 3, *triangles*), we find that the values of S_3 are consistently biased low, an effect that worsens at larger scales. This is due to the finite-volume

[5] Actually, the values of S_3^p and S_4^p we quote are for $\Omega_0 = 1$. For $\Omega_0 = 0.3$, $S_3^p = 2.89$ (Bouchet et al. 1995), which differs by only 0.03 from the value quoted above. We are not aware of a direct analytic calculation of the Ω_0 dependence of S_4, but Bernardeau (1994a) shows that it is very insensitive to Ω_0.

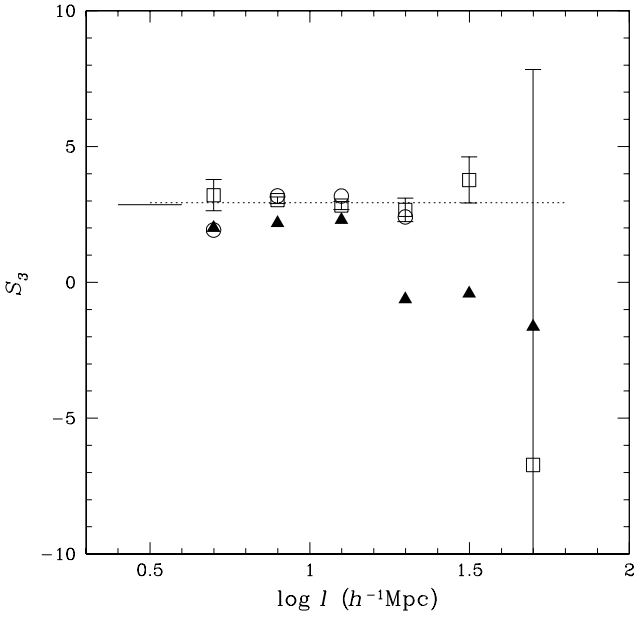

FIG. 3.—Weighted average of S_3 vs. scale of the Edgeworth approximation applied to *IRAS* mock catalogs (*squares*). The average value, $\langle S_3 \rangle = 2.93 \pm 0.09$ (1 σ), is indicated by the dotted line. The circles are the results of the moments method applied to an N-body simulation sampled at 0.01 Mpc^{-3}, which yields an average $\langle S_3 \rangle = 2.90 \pm 0.64$ (1 σ). The solid line on the left is the perturbation theory prediction $S_3^p = 2.86$ for $n = -1$. All three methods agree well. The triangles are the results for the moments method applied to the sparsely sampled mock catalogs. It breaks down at scales larger than $l \sim 16\ h^{-1}$ Mpc because of finite-volume effects (which we do not correct for here) and results in a biased value of S_3.

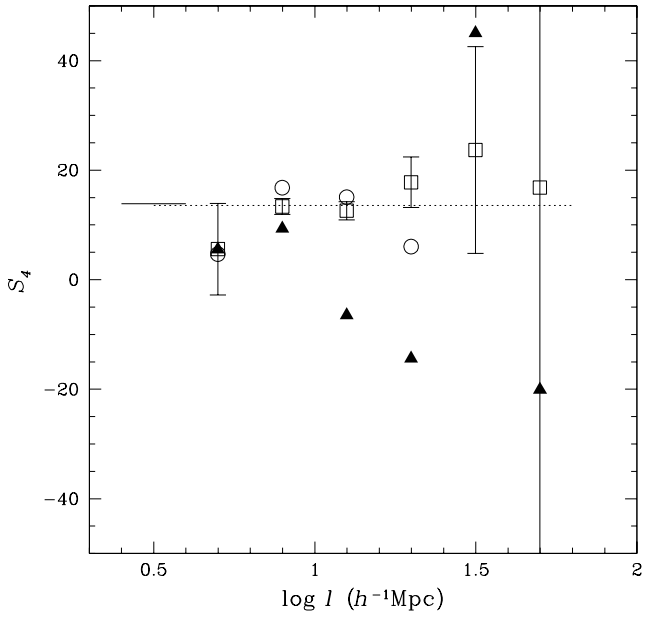

FIG. 4.—S_4 vs. scale for the mock catalogs. Squares denote the weighted average of the Edgeworth approximation applied to mock catalogs, as in Fig 3. The average over scales is $\langle S_4 \rangle = 13.54 \pm 0.53$ (*dotted line*), in agreement with the perturbation theory prediction $S_4^p = 13.89$ (*solid line*) and that of the moments method applied to the full N-body simulation (*circles*). The moments method on sparsely sampled mock catalogs (*triangles*) breaks down on scales larger than $l \sim 10\ h^{-1}$ Mpc.

effect discussed in § 1 and perhaps also to finite-sampling effects as well. We have found that the CPDF for these sparse samples on large scales never clearly reaches the asymptotic exponential tail discussed, e.g., in Colombi et al. (1995), and thus we cannot fit the tail to correct for these effects.

Figure 4 shows results for S_4; the symbols have the same meaning as in Figure 3. The average value of S_4 obtained from the mock catalogs via the Edgeworth approximation is $\langle S_4 \rangle = 13.54 \pm 0.53$ (*squares, dotted line*), which is consistent with the perturbation theory prediction of $S_4 = 13.89$ (*solid line*). The moments method applied to the densely sampled N-body points (*circles*) gives $\langle S_4 \rangle = 12.82 \pm 6.62$, which is very similar to the Edgeworth approximation results (*squares*), albeit again with larger errors, whereas the moments method results from the mock catalog (*triangles*) begin to break down even at very small scales. We conclude that our method gives unbiased estimates of S_3 and S_4, while the moments method is systematically biased low for sparse samples by finite-volume effects, which cannot easily be corrected for.

The last test we perform on N-body simulations is to check the estimation of our error bars, via the method explained in § 2.4. For several specific values of sample size R and smoothing scale l, we draw a series of 50 mock catalogs randomly from the simulation, compute $\tilde{P}(N)$ for each, and fit them to find S_3 and S_4 and their estimated errors in each case. We find in every case that the mean of the estimated errors agrees with the standard deviation of the individual values of S_3 and S_4 to within 10%, which implies that the error estimates are correct in the mean. Of course, this only works when we scale $\mathscr{L}$ by the ratio of χ^2 to the number of degrees of freedom, as discussed in § 2.4; if we do not do this, our errors are overestimated by factors of 2 or 3. However, we emphasize here that our error estimation is not done in a rigorous way; our approach in § 2.4 is empirical at best, and further tests of our errors with simulations with a variety of power spectra are needed to justify these errors fully.

4. RESULTS FOR *IRAS* GALAXIES

Table 2 shows that the best-fit values of σ, S_3, and S_4 are often considerably different from those found by the moments method. Figure 5 shows $\log \sigma \equiv \frac{1}{2} \log \bar{\xi}_2$ versus the smoothing scale, l, for the values found in the third-order Edgeworth expansion fit. The upper panel shows all cases separately, with different symbols representing different sample sizes and lines connecting the points found within each subsample. As the size, R, of the subsample increases, $\sigma(l)$ grows for any given l; more luminous galaxies show stronger clustering than do less luminous galaxies (B93). This luminosity effect agrees well with that of the moments method quantified in B93. However, within each subsample the values trace a power law reasonably well, as does the weighted average given by the squares in the lower panel. The dotted line in the lower panel is a least-squares fit to a power law. The average of the slopes at each value of R is $\gamma/2 = 0.87 \pm 0.08$, crossing unity at an average value of $l_0 = 5.07 \pm 1.45\ h^{-1}$ Mpc, while the moments method (*lower panel, triangles*) yields $\gamma/2 = 0.80 \pm 0.03$ and $l_0 = 5.44 \pm 0.53\ h^{-1}$ Mpc (B93). This is quite reassuring, considering the sensitivity of σ to the order of the fit (Table 2). The large error bar in l_0 is due to its sensitivity on luminosity.

The weighted average values of S_3 and S_4 found by fitting the third-order Edgeworth expansion are summarized in Tables 3 (averaging at a given sample size R) and 4

TABLE 3

S_3 AND S_4 FOR DIFFERENT SUBSAMPLES

MAXIMUM RADIUS (h^{-1} Mpc)	S_3		S_4	
	Moments[a]	Edgeworth[b]	Moments	Edgeworth
23.14.....	1.15	2.30 ± 0.37	0.12	7.09 ± 1.25
37.47.....	2.11 ± 0.14	3.18 ± 0.46	10.6 ± 3.87	10.8 ± 9.62
46.01.....	1.74 ± 0.01	2.31 ± 0.24	1.69 ± 1.00	6.59 ± 0.93
57.34.....	2.19 ± 0.06	2.63 ± 0.11	5.70 ± 0.80	7.39 ± 0.75
72.35.....	1.26 ± 0.06	2.85 ± 0.10	0.86 ± 2.96	2.35 ± 1.92
90.02.....	0.38 ± 0.93	3.15 ± 0.13	-14.7 ± 17.2	8.10 ± 1.66
113.0.....	0.64 ± 1.00	1.98 ± 0.67	-12.2 ± 25.1	-16.9 ± 10.6
140.3.....	-2.55 ± 1.57	2.60 ± 2.36	-30.5 ± 6.75	-7.61 ± 14.1
176.0.....	-8.96 ± 10.8	1.73 ± 1.23	-54.2 ± 58.3	17.4 ± 11.8
219.7.....	-8.71 ± 6.91	1.53 ± 1.53	$-167. \pm 178.$	14.5 ± 43.1

[a] Moments method: equal-weighted average. Errors are 1 σ dispersion.
[b] Results of Edgeworth expansion fit. Weighted average.

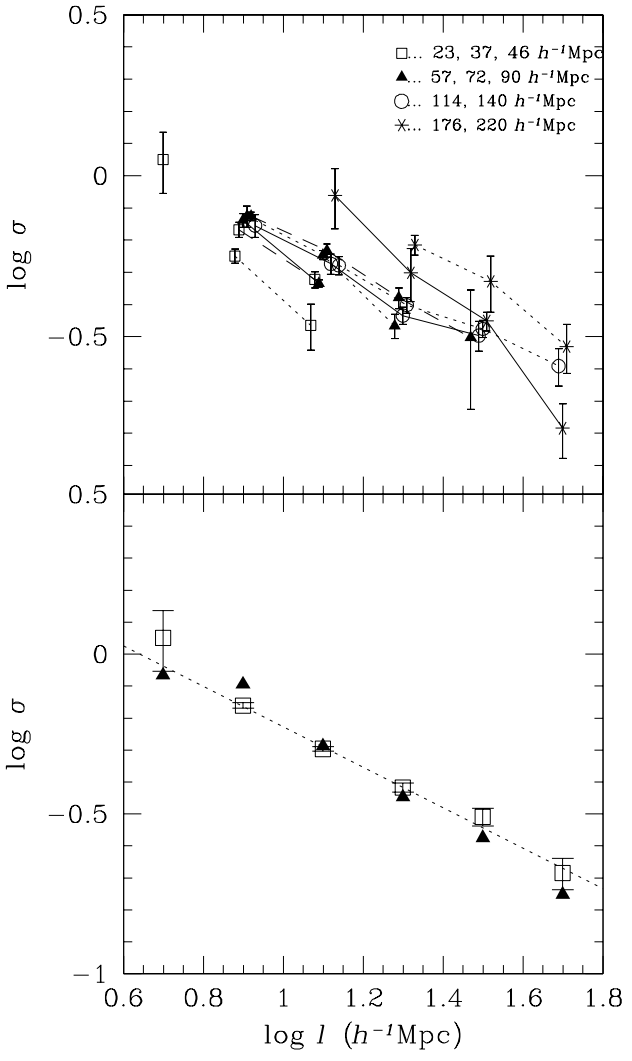

FIG. 5.—A log-log plot of determinations of $\sigma(l)$ vs. l from the third-order Edgeworth expansion fit. In the upper panel, points from each subsample are connected; different symbols denote different sample sizes as shown in the legend. Each symbol is used for several samples: the solid line connects the points for the smallest sample, the dotted line the next, and the dashed line the largest sample that the symbol denotes. The points are slightly staggered to show the error bars. The lower panel shows squares as weighted averages of the top panel. The dotted line is a least-squares fit to the squares, and the triangles in the lower panel are an equal-weighted average of the results from the moments method.

(averaging at a given scale l) and are plotted in Figures 6, 7, and 8. Note that our likelihood method gives meaningful error bars on the values of S_3 and S_4, which enables us to perform a weighted average of our determinations on different scales and from different subsamples, assuming that they are independent of scale.[6]

The figures also show results for the moments method. They are systematically lower than the Edgeworth results because of finite-volume effects. As with the N-body tests described in the previous subsection, we found that on these large scales, the CPDF never reached the asymptotic form that would allow us to correct for these effects (compare with Fry & Gaztañaga 1994, who did perform this correction, but only on scales below 10 h^{-1} Mpc). Error bars for values determined from the moments method can be calcu-

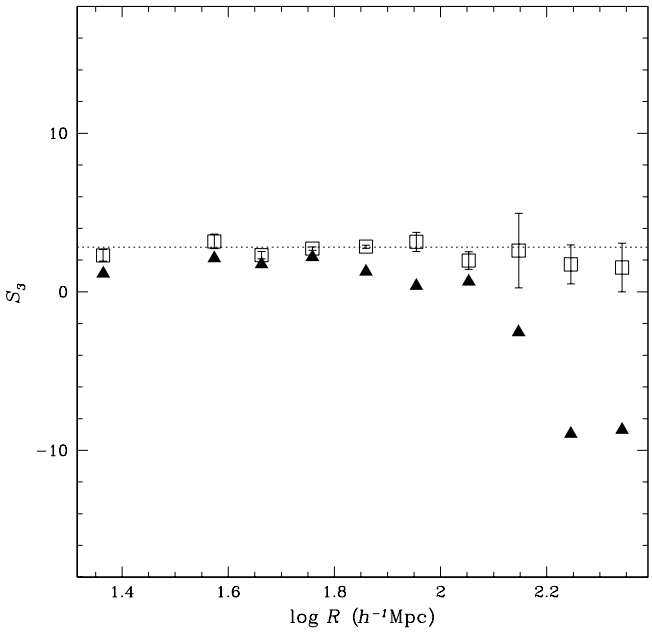

FIG. 6.—Weighted averages of S_3 results from the Edgeworth approximation as a function of subsample size R (*squares*), from Table 3. The triangles are the results of the moments method. The dotted line denotes the global average of the Edgeworth approximation, $\langle S_3 \rangle = 2.83 \pm 0.09$.

[6] There is some covariance due to the fact that the same galaxies are used for the determination of the parameters on different scales; we ignore this effect here.

TABLE 4

S_3 AND S_4 AS A FUNCTION OF SCALE

l (h^{-1} Mpc)	S_3		S_4	
	Moments[a]	Edgeworth[b]	Moments	Edgeworth
5.00	1.15	2.30 ± 0.37	0.12	7.09 ± 1.25
7.92	1.64 ± 0.37	2.87 ± 0.06	4.36 ± 3.57	7.06 ± 0.56
12.6	0.21 ± 2.78	2.67 ± 0.21	3.18 ± 12.7	5.29 ± 1.53
19.9	-0.39 ± 1.15	2.30 ± 1.19	-30.5 ± 21.8	14.6 ± 12.9
31.5	-2.35 ± 3.11	1.02 ± 0.76	-40.2 ± 5.92	-10.0 ± 18.0
50.0	-16.6 ± 9.02	1.17 ± 4.32	$-198. \pm 161.$	$-11.0 \pm 122.$
All.....	-1.76 ± 6.27[c]	2.83 ± 0.06[d]	-31.9 ± 79.0[c]	6.89 ± 0.48[d]
	1.54 ± 0.47[e]		5.8 ± 7.09[e]	

[a] Moments method: equal-weighted average. Errors are 1 σ dispersion.
[b] Results of Edgeworth expansion fit. Weighted average.
[c] Equal-weighted average of all values.
[d] Weighted average of all values. Note that our final quotes are $\langle S_3 \rangle = 2.83 \pm 0.09$ and $\langle S_4 \rangle = 6.89 \pm 0.68$ (see discussion in § 4).
[e] Equal-weighted average of all positive values.

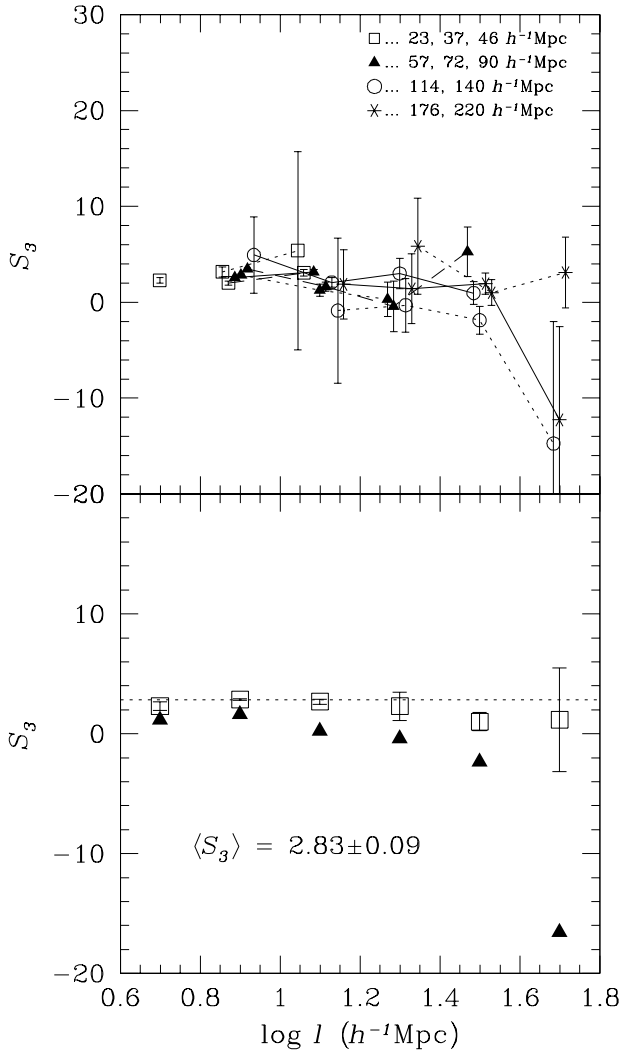

FIG. 7.—All determinations of S_3 as a function of scale (*top panel*). As in Fig. 5, different symbols indicate different subsamples, with lines connecting the values within the same subvolume. The bottom panel shows weighted averages of the Edgeworth approximation results as squares; the averages of the results of the moments method are indicated by triangles. The dashed line is the global average of the Edgeworth approximation results, $\langle S_3 \rangle = 2.83 \pm 0.09$.

lated (Szapudi & Colombi 1996) but are quite complicated. Following B93, we use the standard deviation of determinations of S_3 and S_4 as our error bar for the moments method, including only positive values.

The Edgeworth approximation yields values of S_3 and S_4 (Figs. 6–8, *squares*), which show no statistically significant dependence on R or l, consistent with the scale-invariant hypothesis (see discussion below). Without finite-volume corrections, this scale invariance is not apparent from the moments results. This is not an issue with the Edgeworth method; it is quite insensitive to the tail of the CPDF, and thus no correction for finite-volume effects is needed.

We find a global average of $\langle S_3 \rangle = 2.83 \pm 0.06$,[7] which is appreciably larger than the value $\langle S_3 \rangle = 1.5 \pm 0.5$ found in B93. This is consistent with the bias in the moments method that we found in § 3; we showed there that the Edgeworth method is unbiased, and we therefore believe that our determination of $\langle S_3 \rangle$ for *IRAS* galaxies supersedes that of B93. Our results are in better agreement with the moments methods results for *IRAS* from Fry & Gaztañaga (1994), who found $S_3 = 2.1 \pm 0.3$ and $S_4 = 7.5 \pm 2.1$, in the range 3–10 h^{-1} Mpc, and Meiksin et al. (1992) from the angular distribution of *IRAS* galaxies ($S_3 = 2.2 \pm 0.2$ and $S_4 = 10 \pm 3$ in the range 4–10 h^{-1} Mpc).[8]

Our result uses the third-order Edgeworth expansion; if we use the second-order expansion, we find $\langle S_3 \rangle = 2.80 \pm 0.11$, which is consistent with the value from the third-order fit. In both cases, the average is dominated by the point with the smallest errors, $\langle S_3 \rangle = 2.87 \pm 0.06$ at 8 h^{-1} Mpc.

Given the estimated errors on S_3 for each value of R and l, we can do an a posteriori test of the hypothesis that S_3 is independent of subsample and scale by computing the χ^2-like statistic:

$$\mathscr{R} = \sum_{\text{realizations } i} \frac{(S_{3,i} - \langle S_3 \rangle)^2}{\sigma^2_{S3,i}}, \qquad (24)$$

where the sum is over all different values of R and l. We find that $\mathscr{R}$ exceeds the number of measurements of S_3 by a

[7] This error bar is smaller than our final quoted value of 0.09 ; see discussion below.

[8] Note, however, that one does not expect the angular and spatial S_N to be identical (see also Bernardeau 1995).

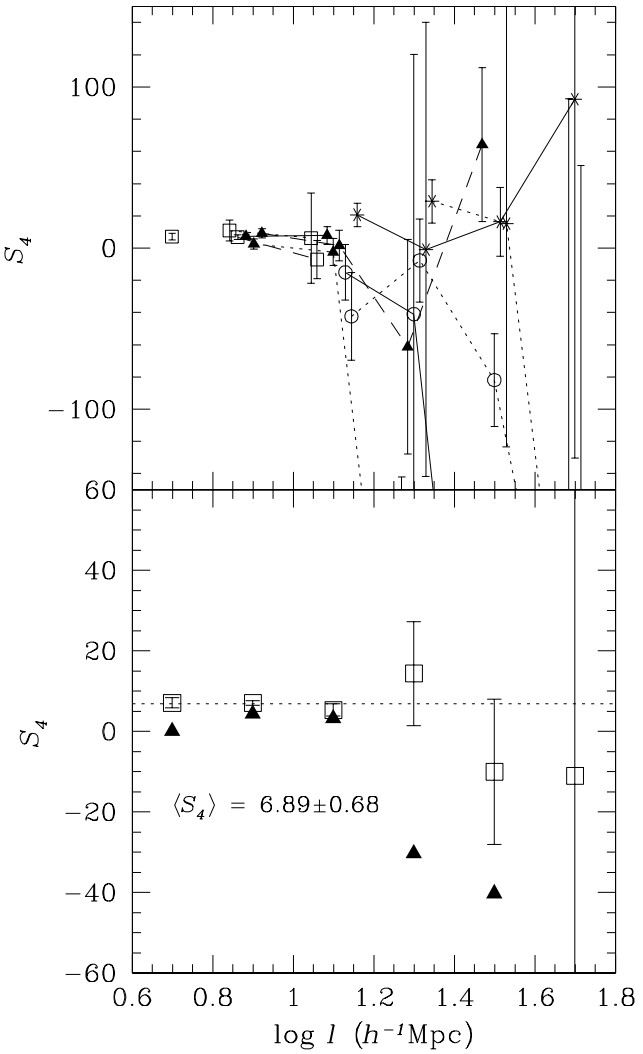

FIG. 8.—S_4 as a function of scale. Symbols have the same meaning as in Fig. 7.

factor of 2. This is due to several effects: cosmic variance, the approximation we have made that the errors in S_3 determined at different scales from the same data are statistically independent, and possible real scale dependence of S_3 caused by higher order effects (see Colombi et al. 1996). Our final error bar should reflect this increased scatter, and so we multiply the error on $\langle S_3 \rangle$ by $\mathscr{R}^{1/2} = 1.4$, which yields $\langle S_3 \rangle = 2.83 \pm 0.09$. It would be interesting to separate out these effects with a $n = -2$ simulation, in which these higher order effects should be more important (Colombi et al. 1996); this is work for the future.

Figure 8 shows the determination of S_4 as a function of scale. For scales larger than $\log l = 1.3$, S_4 becomes very uncertain, with large error bars. However, the weighted average values of S_4 in the bottom panel stay close to the total average value of $\langle S_4 \rangle = 6.89 \pm 0.48$, with error bars overlapping that value at all scales. We carried out the χ^2 test of equation (24) for S_4 as well, finding $\mathscr{R} = 2$ again. We thus also multiply our quoted error on $\langle S_4 \rangle$ by 1.4, which yields $\langle S_4 \rangle = 6.98 \pm 0.68$. This again is larger than, albeit statistically consistent with, the moments method results of $\langle S_4 \rangle = 4.4 \pm 3.7$ (B93) and is in agreement with Meiksin et al. (1992) and Fry & Gaztañaga (1994), quoted above.

Gaztañaga (1992) used the moments method to find $\langle S_3 \rangle = 1.94 \pm 0.07$ for optically selected galaxies. Gaztañaga (1992) and B93 claim that the lower value of S_3 for *IRAS* galaxies can be attributed to the underrepresentation of *IRAS* galaxies in dense cluster cores (see also Strauss et al. 1992). As a test of this, B93 gave extra weight to the *IRAS* clusters to match the overdensities seen in optically selected galaxies; they found the S_N to be quite sensitive to this: $\langle S_3^b \rangle = 3.71 \pm 0.95$ and $\langle S_4^b \rangle = 23.6 \pm 12.1$. This demonstrates the high sensitivity of the moments method to dense clusters; the moments are heavily weighted by the tail of the CPDF, and this effect is even more important for S_4 than for S_3. This sensitivity is very dangerous, given the fact that the tail is generally hard to measure with accuracy, as we have seen. We have fit the Edgeworth model to the CPDF of these cluster-boosted counts and found $\langle S_3^b \rangle = 2.65 \pm 0.09$ and $\langle S_4^b \rangle = 7.79 \pm 0.67$, which are within 2 standard deviations of the unboosted results above. This is as expected; boosting the clusters only affects the CPDF in the tail, and therefore this has only a small effect on our fits.

One might argue that this result is misleading; if our Edgeworth model is a good fit to the full CPDF before the cluster boosting, it *cannot* be a good fit afterward because the tail has changed dramatically, even though the boosting has very little effect on the rest of the CPDF. Clearly, the moments method and our method cannot agree in both cases, independent of issues of finite volume effects. With our method, S_3 and S_4 are determined from a fit to that part of the CPDF that is close to mean density, and therefore is not highly nonlinear, while the moments method is quite sensitive to the nonlinear tail. Thus our method can measure S_3 and S_4 in the weakly nonlinear regime, even when strong clustering is present.

The effective power-law index for *IRAS* galaxies is $n = -1.4$ (Fisher et al. 1993), which would predict that $S_3 = 3.26$ and $S_4 = 22.4$. Why do our results differ from these values? If the *IRAS* galaxy distribution were biased with respect to the underlying mass, one would expect that the skewness and kurtosis would be systematically affected. The linear bias model, $\delta_g = b\delta_M$, where δ_g is the observed galaxy density field and δ_M is the underlying mass density contrast, predicts $S_{3,g} = S_{3,M}/b$ and $S_{4,g} = S_{4,M}/b^2$. However, as Fry & Gaztañaga (1993) point out, we cannot consider high-order correlations without also considering the possibility of high-order bias (Gaztañaga & Frieman 1994; Juszkiewicz et al. 1995):

$$\delta_g = f(\delta) = \sum_{k=1}^{\infty} \frac{b_k}{k!} \delta_M^k \,. \tag{25}$$

This leads to

$$S_{3g} = S_{3M}/b_1 + 3b_2/b_1^2 + \mathcal{O}(\langle \delta^2 \rangle) \tag{26}$$

$$S_{4g} = S_{4M}/b^2 + 12S_{3M}\, b_2/b_1^3 + 4b_3/b_1^3 + 12b_2^2/b_1^4 + \mathcal{O}(\langle \delta^2 \rangle) \,. \tag{27}$$

Thus, without external information on the detailed form of the biasing relation, we cannot make a direct comparison of our results with those from perturbation theory.

5. CONCLUSIONS

We have measured the count probability distribution function via the counts-in-cells method for 10 volume-limited subsamples of the *IRAS* 1.2 Jy redshift survey,

exactly as in B93. There are various approaches to measure the skewness, S_3, and kurtosis, S_4, of the probability distribution function of the underlying density field. B93 calculated these quantities for this sample using the moments method. They found scale invariance of S_3 to $l \sim 25\ h^{-1}$ Mpc, with an average value of $S_3 = 1.5 \pm 0.5$. However, the moments method is very sensitive to the high-density tail of the CPDF, which makes the values of S_3 and S_4 sensitive to finite-volume and finite-sampling effects. These effects can be corrected for (Fry & Gaztañaga 1994; Colombi et al. 1995; Szapudi & Colombi 1996; Szapudi et al. 1996), at least in the strongly nonlinear regime with dense sampling. We work here with a very sparse redshift survey in the weakly nonlinear region ($\bar{\xi}_2 < 1$) and find that the CPDF never properly reaches the asymptotic limit that allows one to correct for finite-volume effects. We propose a method less sensitive to the tails of the CPDF, a maximum likelihood fit of the Edgeworth expansion convolved with a Poissonian, to the observed CPDF. The Edgeworth expansion is valid only in the weakly nonlinear regime ($\sigma < 1$); unlike the moments method, it cannot be applied on very small scales.

We have tested our method with *IRAS* mock catalogs extracted from *N*-body simulations; we find that the derived values of S_3 and S_4 are consistent with the analytic predictions from perturbation theory, as well as from the moments method as derived from densely sampled *N*-body points. Moreover, our estimated errors are consistent with the scatter in S_3 and S_4 seen in multiple realizations of the sample. The results from the moments method in these sparse mock catalogs are systematically biased low, especially on large scales, owing to finite-volume effects. Hence, we conclude that the Edgeworth approximation is much more reliable and robust than the moments method is, especially in sparse samples and in the weakly nonlinear regime, where there is no simple method to correct for these effects.

The resulting values of S_3 and S_4 are found to be $\langle S_3 \rangle = 2.83 \pm 0.09$ and $\langle S_4 \rangle = 6.89 \pm 0.68$, which are significantly higher than the results of B93 but are consistent with Meiksin et al. (1992) and Fry & Gaztañaga (1994). These results are quite insensitive to the fact that *IRAS* galaxies are underrepresented in cluster cores. Both S_3 and S_4 are independent of scale within the errors from 5 to 50 h^{-1} Mpc.

We have shown that the data are consistent with the scale-invariant hypothesis. It would be very interesting to compare these results with those from various specific models with non-Gaussian initial conditions, to see at what level we might be able to rule them out.

Application of the Edgeworth approximation to optical samples should be interesting, especially since previous work has shown discrepancies with the *IRAS* sample, attributed to the underrepresentation of *IRAS* galaxies in clusters. It would also be interesting to apply this technique to angular surveys such as the APM galaxy sample, where we could carry this technique out to appreciably higher order. We also look forward to applying this technique on the spectroscopic and photometric data of the Sloan Digital Sky Survey (see Gunn & Weinberg 1995), which will allow us to probe appreciably larger spatial scales.

There is also further work to be done on the method itself. Our understanding of the errors and covariances in the CPDF, and therefore the errors in our derived parameters, is poor, and thus our final errors are not rigorously justified. As we have seen in § 4, the χ^2 test (eq. [24]) suggests that our method of obtaining error bars can hide interesting higher order effects. In particular, without good a priori errors, we cannot do a proper test of goodness of fit of our model. Further analytical work in this direction is needed, together with more extensive tests with simulations over a wider range of conditions.

We thank R. Juszkiewicz and D. Weinberg for important discussions at the outset of this project, E. Gaztañaga, S. Colombi, and an anonymous referee for useful comments, and D. Weinberg for the *N*-body simulations used in this paper. M. A. S. gratefully acknowledges the support of an Alfred P. Sloan Foundation Fellowship, as well as the support of NASA Astrophysical Theory Grant NAG 5-2882. R. S. J. K. acknowledges the support of an Assistant in Research Tuition Award from Princeton University, and NSF grant AST 93-15368.

REFERENCES

Amendola, L. 1994, ApJ, 430, L9
Balian, R., & Schaeffer, R. 1988, ApJ, 335, L43
———. 1989, A&A, 220, 1
Bernardeau, F. 1992, ApJ, 392, 1
———. 1994a, ApJ, 433, 1
———. 1994b, A&A, 291, 697
———. 1995, A&A, 301, 309
Bernardeau, F., & Kofman, L. 1995, ApJ, 443, 479
Borgani, S. 1995, Phys. Rep., 251, 1
Bouchet, F. R., Colombi, S., Hivon, E., & Juszkiewicz, R. 1995, A&A, 296, 575
Bouchet, F. R., Juszkiewicz, R., Colombi, S., & Pellat, R. 1992, ApJ, 394, L5
Bouchet, F. R., Strauss, M. A., Davis, M., Fisher, K. B., Yahil, A., & Huchra, J. P. 1993, ApJ, 417, 36 (B93)
Coles, P., & Jones, B. J. T. 1991, MNRAS, 248, 1
Colombi, S., Bernardeau, F., Bouchet, F. R., & Hernquist, L. 1997, MNRAS, 287, 241
Colombi, S., Bouchet, F. R., & Hernquist, L. 1996, ApJ, 465, 14
Colombi, S., Bouchet, F. R., & Schaeffer, R. 1994, A&A, 281, 301
———. 1995, ApJS, 96, 401
Cramér, H. 1946, Mathematical Methods of Statistics (Princeton: Princeton Univ. Press)
da Costa, L. N., Pellegrini, P., Davis, M., Meiksin, A., Sargent, W., & Tonry, J. 1991, ApJS, 75, 935
Fisher, K., B., Davis, M., Strauss, M., A., Yahil, A., & Huchra, J. P. 1993, ApJ, 402, 42
Fisher, K. B., Huchra, J. P., Davis, M., Strauss, M. A., Yahil, A., & Schlegel, D. 1995, ApJS, 100, 69
Fry, J. N. 1984a, ApJ, 277, L5
———. 1984b, ApJ, 279, 499
Fry, J. N., & Gaztañaga, E. 1993, ApJ, 413, 447
———. 1994, ApJ, 425, 1
Fry, J. N., & Scherrer, R. J. 1994, ApJ, 429, 36
Gaztañaga, E. 1992, ApJ, 398, L17
———. 1994, MNRAS, 268, 913
———. 1995, ApJ, 454, 561
Gaztañaga, E., & Frieman, J. A. 1994, ApJ, 437, L13
Gaztañaga, E., & Yokoyama, J. 1993, ApJ, 403, 450
Gunn, J. E., & Weinberg, D. H. 1995, in Wide-Field Spectroscopy and the Distant Universe, ed. S. J. Maddox & A. Aragón-Salamanca (Singapore: World Scientific), 3
Hivon, E., Bouchet, F. R., Colombi, S., & Juszkiewicz, R. 1995, A&A, 298, 643
Huchra, J. P., Davis, M., Latham, D., & Tonry, J. 1983, ApJS, 52, 89
Juszkiewicz, R., Bouchet, F. R., & Colombi, S. 1993, ApJ, 412, L9
Juszkiewicz, R., Weinberg, D. H., Amsterdamski, P., Chodorowski, M., & Bouchet, F. R. 1995, ApJ, 442, 39
Kofman, L., Bertschinger, E., Gelb, J. M., Nusser, A., & Dekel, A. 1994, ApJ, 420, 44
Lahav, O., Itoh, M., Inagaki, S., & Suto, Y. 1993, ApJ, 402, 387
Łokas, E. L., Juszkiewicz, R., Weinberg, D. H., & Bouchet, F. R. 1995, MNRAS, 274, 730
Meiksin, A., Szapudi, I., & Szalay, A. S. 1992, ApJ, 394, 87
Park, C. 1990, Ph.D. thesis, Princeton University
Peebles, P. J. E. 1980, The Large-Scale Structure of the Universe (Princeton: Princeton Univ. Press)

Press, W. H., Flannery, B. P., Teukolsky, S. A., & Vetterling, W. H. 1992, Numerical Recipes, The Art of Scientific Computing (2d ed.; Cambridge: Cambridge Univ. Press)
Protogeros, Z. A. M., & Weinberg, D. H. 1997, ApJ, 489, 457
Scherrer, R. J., & Bertschinger, E. 1991, ApJ, 381, 349
Strauss, M. A., Davis, M., Yahil, A., & Huchra, J. P. 1992, ApJ, 385, 421
Strauss, M. A., & Willick, J. A. 1995, Phys. Rep., 261, 271
Szapudi, I., & Colombi, S. 1996, ApJ, 470, 131
Szapudi, I., Dalton, G. B., Efstathiou, G., & Szalay, A. S. 1995, ApJ, 444, 520
Szapudi, I., Meiksin, A., & Nichol, R. C. 1996, ApJ, 473, 15
Szapudi, I., & Szalay, A. S. 1996, ApJ, 459, 504
Szapudi, I., Szalay, A. S., & Boschan, P. 1992, ApJ, 390, 350
Ueda, H., & Yokoyama, J. 1996, MNRAS, 280, 754
Zeldovich, Y. B. 1970, A&A, 5, 84